Proceedings World Geothermal Congress 2010
Bali, Indonesia, 25-29 April 2010

Dynamic Modelling and Simulation of an Organic Rankine Cycle Unit of a Geothermal Power Plant

M. Imroz Sohel[1*], Susan Krumdieck[1], Mathieu Sellier[1], Larry J. Brackney[2]

[1] Department of Mechanical Engineering, University of Canterbury, Christchurch, New Zealand.

[2] Department of Electrical and Computer Engineering, University of Canterbury, Christchurch, New Zealand.

* Corresponding author. Email: mso32@student.canterbury.ac.nz; mohammed.imroz.sohel@gmail.com

Tel: +64 3 3642987 ext 7243; Fax: +64 3 3642078;

Keywords: Geothermal power, dynamic modelling, binary cycle, ORC.

ABSTRACT

This article presents a dynamic model of a 5.4 MW binary cycle unit of a geothermal power plant. The plant is an Organic Rankine Cycle (ORC) where pentane is used as the motive fluid and it is powered by the separated brine from the geothermal fluid. It is found that the inlet brine properties including brine mass flow rate, and the ambient air temperature are the two most important parameters influencing the plant performance. Specifically, the plant performance is highly dependent on the ambient air temperature as the ORC uses air-cooled condenser. Moreover, the inlet brine property changes less significantly with respect to time compared to the ambient air temperature. Simulation has been carried out where, brine inlet properties and ambient air temperature are fed as inputs to the computer model. The simulated plant performance has been compared with the actual plant performance data. It has been found that the developed model is very competent in predicting plant performance. The average percentage error of the theoretical and the observed power outputs remain within 5%.

1. INTRODUCTION

Geothermal plants have a large number of parts involving an enormous number of flow recirculations and splitting, and connections of several subsystems. The overall plant behaviour, both static and dynamic, cannot be simply inferred from that of its components, rather it is essentially determined by their interaction (Casella 1999). Although a wide range of literature is available on the steady state operation of a geothermal power plant, dynamic models are not very common. Dynamic models are very useful in two areas, firstly, in controlling and monitoring the system for transient conditions, particularly when the load demand or the quality or flow of geothermal fluid suddenly changes (Wei et al. 2008). It is necessary to keep the proportion of liquid and vapour phases in the condenser and evaporator within acceptable ranges to avoid stalling or temperature shocks. Secondly, it is very convenient for the plant operators to know what the power output could be under given ambient conditions, plant parameters and geothermal fluid flow rate. The plant operators need to inform the dispatcher beforehand how much power they can produce as the price of the electricity depends on it. Normally, there is a huge penalty for the plant owners, if they produce more than promised to avoid grid overload (Pritchard 2002). A dynamic model can ease this problem by predicting power output in advance with high accuracy.

This paper presents a dynamic model of a 5.4 MW binary cycle unit of a geothermal power plant. The brine inlet properties and the ambient air temperature are used as the inputs to the model. The developed dynamic model meant for predicting the plant performance depending on weather condition and brine inlet properties. Therefore, transient phenomenons i.e. starting up or shutting down processes are not discussed here. These are done manually in the plant. The following section introduces the plant. Modelling of each of the component then follows. Results and discussions are presented in the last section of the paper.

2. THE ORC UNIT

Figure 1 shows the process flow diagram of the ORC unit. It is powered by brine from the geothermal fluid. The brine, which is at about 205°C, passes through the vaporizer-separator providing heat for the ORC unit. Pentane taking heat from the brine changes its phase from liquid to vapor in the vaporizer then superheated in the separator. It is then passes through the turbine producing work. Then it passes through a recuperator before being cooled by an air-cooled condenser. The recuperator recovers some of the heat from the pentane vapor coming from the turbine reducing the heat load in the condenser. The pentane liquid after the cycle-pump passes through the recuperator, where it is heated to an elevated temperature. Then the pentane liquid enters the vaporizer completing the cycle. Figure 2 presents the *T-s* plane presentation of the cycle.

2.1 Modeling of the Components

Following sections present modeling of each of the components. The components are modeled separately and then they are connected to form the model of the geothermal power unit. The model developed for this study were solved using commercial software packages Matlab/Simulink® and gPROMS® (MathWorks 2008; PSE 2008).

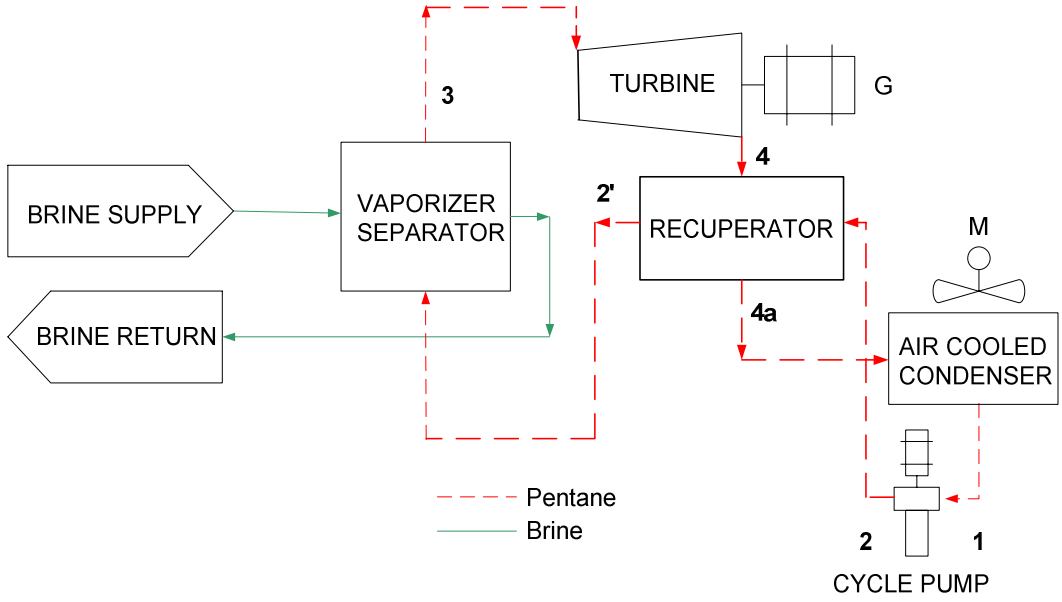

Figure 1: Process diagram of the ORC unit

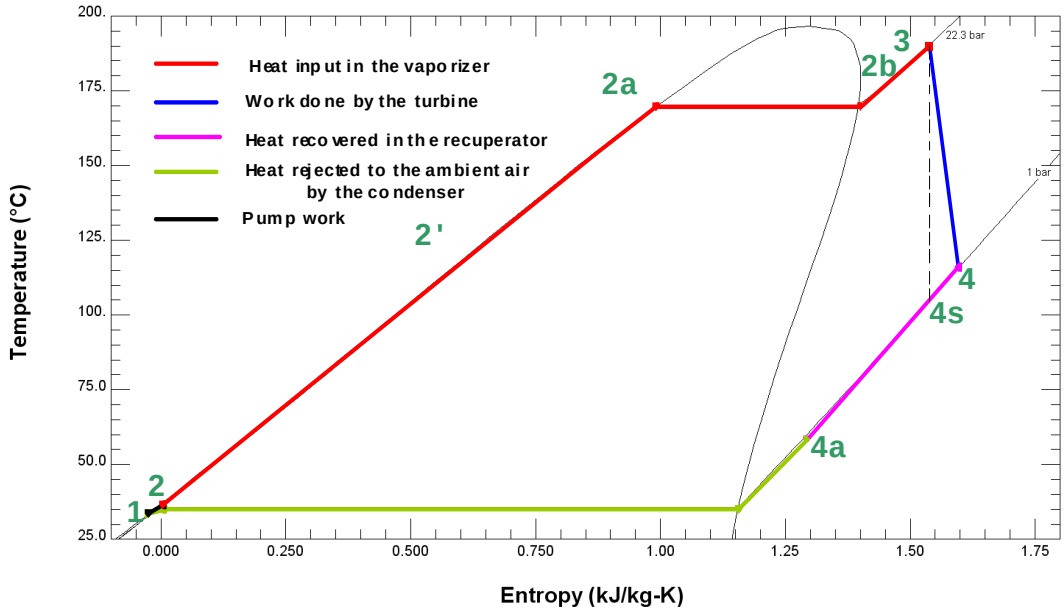

Figure 2: *T,s*-diagram of the ORC

2.2 The vaporizer-separator model

Some of the authors in the literature i.e. (Wei et al. 2008) have used discretization techniques to dynamically model vaporizers and condensers which take into account temperature gradient along the geometry of a heat exchanging device. However, models based on lumped parameters by some other authors i.e. (Bai et al. 2004) have yielded reasonably high accuracy with appropriate assumptions. It also avoids complicated calculations. If Biot number is less than 0.1 then the lumped capacitance method can be applied with reasonably accuracy(Holman 1992).

Figure 3 shows a schematic diagram of the vaporizer-separator. A simplified view of the vaporizer and a simplified view of the separator are presented in Figure 4 and Figure 5, respectively.

Both the vaporizer and the separator are shell and tube type heat exchangers with brine on the tube side and working fluid (pentane) on the shell side. The vaporizer is fitted with a level control arrangement. There are two sensors fixed to two different elevations of the vaporizer. The bottom one is assigned to 0 and top one is 100. The pentane level is kept within this operating range, and if the pentane level goes below 0 or above 100, a shut down sequence is initiated. The vaporizer level indicates quantity (mass) pentane inside the vaporizer/separator know as hold up mass.

The following assumptions were made for the vaporizer model:

1. The temperature and pressure are assumed to be the same for the vaporizer and the lower half of

the separator. Therefore, the holdup mass of pentane vapor in the lower part of separator is added to the total holdup mass of pentane in the vaporizer.

2. There is a temperature gradient in the separator along the diameter towards the vertical direction. To approximate it, the upper half of the separator is assumed responsible for the superheating.
3. The holdup mass of pentane in the upper half of the separator is negligible.
4. Heat capacity of the material of the vaporizer/separator is negligible. The Biot number of combined vaporizer and separator is 0.00433 (<0.1) which justifies such assumption (Holman 1992).
5. Heat loss to the environment is negligible.

Using the above assumptions, the heat balance equation of the vaporizer in lumped parameter form is given as follows:

$$\frac{d}{dt}(M_l h_{2a} + M_v h_{2b}) = \dot{m}_2 h_2 + Q^V - \dot{m}_{2b} h_{2b} \quad (1)$$

Here, M_l is the holdup mass of liquid; h_{2a} is the enthalpy of the holdup liquid; M_v is the holdup mass of vapour; h_{2b} is the enthalpy of the holdup vapour; $\dot{m}_2$ is the mass flow of inlet liquid; h_2 is the enthalpy of inlet liquid; Q^V is the heat input in the vaporizer and lower half of theseparator; and $\dot{m}_{2b}$ is the mass flow of outlet vapour.

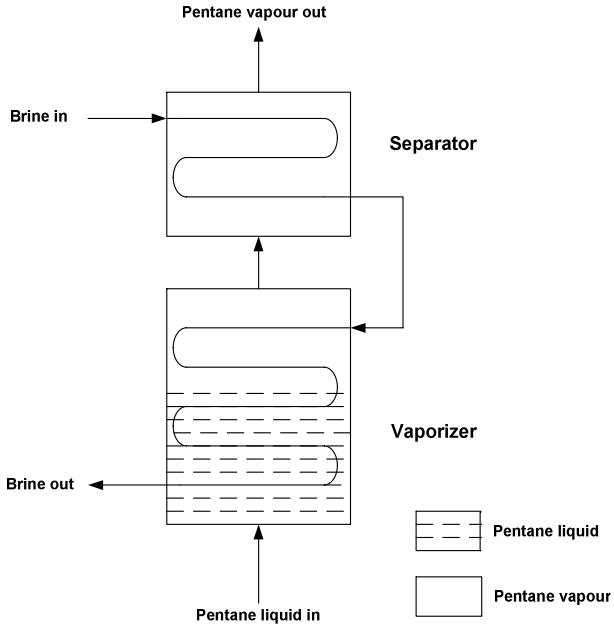

Figure 3: Schematic diagram of the vaporizer and separator

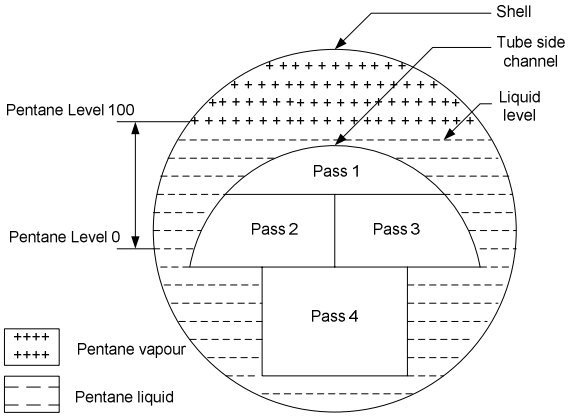

Figure 4: Simplified cross-sectional view of the vaporizer

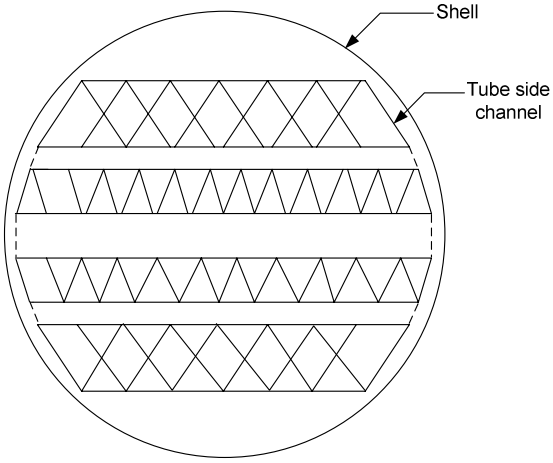

Figure 5: Simplified cross sectional view of the separator

The heat transfer from the brine to the working fluid is calculated from the following equation.

$$Q^T = U^T A^T \Delta t_m^T \quad (2)$$

Where, U^T is the overall heat transfer coefficient, A^T is the total effective heat transfer area of the vaporizer and the separator and Δt_m^T is the combined log mean temperature deference (LMTD) and calculated as:

$$\Delta t_m^T = \frac{(T_{i,B} - T_3) - (T_{o,B} - T_{2a})}{\ln \frac{(T_{i,B} - T_3)}{(T_{o,B} - T_{2a})}} \quad (3)$$

Unfortunately, it is not possible to calculate the LMTD for the vaporizer and the separator separately. In the ORC cycle, the outlet temperature of the brine from the separator before entering the vaporizer is not known. Therefore, the LMTD for the combined vaporizer and separator was used.

The value of the overall heat transfer coefficient for the combined vaporizer and separator is calculated using the following approximated equation as presented by Bai et al. (Bai et al. 2004) taken from experimental results presented by Nakaoka and Uehara (Nakaoka and Uehara 1988).

$$U^T = U_S^T (\dot{m}_B^T / \dot{m}_{S,B}^T)^{0.5} \quad (4)$$

Here, $\dot{m}_B^T$ is the brine mass flow, U_S^T is the standard heat transfer coefficient and $\dot{m}_{S,B}^T$ is the standard brine mass flow.

At first, the total heat transfer is calculated, then it is divided between the separator and the vaporizer in the same ratio as observed, Q^V=87.2% and Q^S=12.8% of Q^T.

Equation 4 is an approximated relationship devised from experimental data from a shell and plate heat exchanger. However, in the ORC unit, the vaporizer and separator are shell and tube type. Therefore, to increase the accuracy of the calculation, iteration was carried out.

At first using equation (4), U^T was calculated. Using equation (2), Q^T was calculated. Now, brine side heat transfer,

$$Q^T = \dot{m}_B c_p (T_{i,B} - T_{o,B}) \quad (5)$$

From the above equation, keeping $T_{i,B}$ constant, the value of $T_{o,B}$ can be calculated. Using the new value of $T_{o,B}$, the value of Δt_m^T, can be calculated and so forth.

From conservation of mass in the vaporizer we get,

$$\frac{d}{dt}(M_l + M_v) = \dot{m}_2 - \dot{m}_{2b} \quad (6)$$

Where, M_l and M_v are holdup masses of pentane liquid and vapor in the vaporizer and lower half of the separator, respectively. $\dot{m}_2$ is the pentane liquid mass flow to the vaporizer and $\dot{m}_{2b}$ is the pentane vapor flow from the vaporizer.

The combined space inside the vaporizer and the separator is constant. As the holdup mass of the upper half is ignored, the following relationships can be expressed for the vaporizer:

$$V_T = V_V + 0.5V_S \quad (7)$$

$$V_T = V_v + V_l \quad (8)$$

$$V_l = M_l / \rho_l \quad (9)$$

$$V_v = M_v / \rho_v \quad (10)$$

Here, V_T is the total volume of the space inside the vaporizer and the lower half of the separator, V_V is the volume of the space inside the vaporizer and V_S is the volume of the space inside the separator. V_l is the volume of the liquid pentane inside the vaporizer and V_v is the volume of the vapor on top of the pentane liquid level and the space of the lower half of the separator. ρ_l and ρ_v are the density of saturated liquid and saturated vapor.

The mass flow of pentane vapor depends on the amount of heat given to the fluid from the brine. From energy balance, the following equation can be derived:

$$\dot{m}_{2b} = \frac{Q^V - \dot{m}_2 (h_{2a} - h_2)}{L_v} \quad (11)$$

Where, L_v is the latent heat of vaporization. The outlet temperature from the separator is calculated depending on the state of the pentane vapor. If $h_{2b} = h_{sat}$ then:

$$T_3 = T_{sat} + \frac{Q^S}{cp\,\dot{m}_{2b}} \quad (12)$$

If $h_{2b} < h_{sat}$ then

$$T_3 = T_{sat} + \frac{Q^S - m_{2b}(h_{sat} - h_{2b})}{cp\,\dot{m}_{2b}} \quad (13)$$

If $h_{2b} > h_{sat}$ then

$$T_3 = T_{sat} + \frac{Q^S + m_{2b}(h_{2b} - h_{sat})}{cp\,\dot{m}_{2b}} \quad (14)$$

Here, the suffix *sat* stands for saturation. All the physical properties needed for equations 9 - 14 are taken from (REFPROP 2007).

$$h_3 = h_{2b} + \frac{Q^S}{\dot{m}_{2b}} \quad (15)$$

Figure 6 represents a simplified view of Figure 4 with an explanation of various parameters. The line *AC* represents the level of pentane in the vaporizer. The volume of vapor above this line can be calculated by multiplying area bounded by *ABC* with the length of the vaporizer. This area is equal to the area bounded by *ABCO* minus the area of the triangle *ACO*.

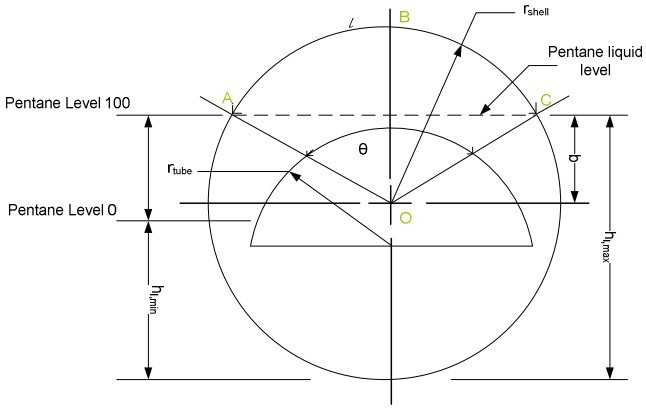

Figure 6: Simplified cross sectional view of the vaporizer

It can be easily shown that for a pentane level higher than or equal to the top of the tube channel, the height of the pentane level from the bottom of the shell, h_l, can be calculated from the following equation:

$$V_l = (V^S - V_{tube}) - (\frac{1}{2} r_{shell}^2 (2\cos^{-1}((h_l - r_{shell})/r_{shell})) - (h_l - r_{shell})\sqrt{(2h_l r_{shell} - h_l^2)})\, l_V \quad (16)$$

If the liquid pentane level is lower than the top of the tube channel, h_l can be calculated iteratively from the following equation:

$$V_l = (V^S - V_{tube}) - (\frac{1}{2} r_{shell}^2 (2\cos^{-1}((h_l - r_{shell})/r_{shell})) - (h_l - r_{shell})\sqrt{(2h_l r_{shell} - h_l^2)})\, l_V + (\frac{1}{2} r_{tube}^2 (2\cos^{-1}((h_l - r_{tube})/r_{tube})) - (h_l - r_{tube})\sqrt{(2h_l r_{tube} - h_l^2)})\, l_V \quad (17)$$

Where, h_l is the height of the pentane liquid level from the bottom of the vaporizer, r_{shell} is the internal radius of the shell, r_{tube} is the outer radius of the tube, V_{tube} is the volume (external) of the tube side channel and l_v is the length of the vaporizer.

The liquid level, h_l is explained in Figure 6:

$$h_l = r_{shell} + b \quad (18)$$

The percentage of liquid level is calculated from the following equation,

$$l_{\%} = \frac{(h_l - h_{l,\min})}{(h_{l,\max} - h_{l,\min})} \times 100 \quad (19)$$

Equations 7 - 10 and 16-17 are pure algebraic equations and are a part of a system of differential equations forming a typical higher index problem. An index greater than 1 implies that there are algebraic relations between dynamic variables. A higher index problem can be solved by reducing its index to 1 using dummy derivatives (Mattsson and Siiderlind 1993). gPROMS can solve a high *index* automatically. However, one must provide consistent initial conditions to start simulation. The gPROMS model was exported to Simulink via gO:Simulink interface.

2.3 The turbine model

The response time of a turbine can be in the order of 10-20 s (Jurado et al. 2003) to 1-3 minutes. The available data of the plant operation is for one-hour interval so we are interested in plant performance where unit time is 60 min or an hour. Therefore, the turbines can be assumed to have static behaviour with respect to the unit time of our interest. Ou Bai et al. and Wei et al. (Bai et al. 2004; Wei et al. 2008) have used such static representation of turbine models used for dynamic modelling of binary cycles.

Figure 1 presents *T-s* presentation of a Rankine cycle with the process 3-4_s as an ideal turbine. The work done by an ideal turbine can be calculated knowing the state points 3 and 4_s and calculated as:

$$W_T = \dot{m}(h_3 - h_{4s}) \quad (20)$$

Where, W_T is work done by the turbine, $\dot{m}$ is the mass flow rate of the working fluid through the turbine, h_3 is the enthalpy of the working fluid at point 3 and h_{4s} is the enthalpy of the working fluid at the outlet of the turbine at isentropic condition.

For a reversible adiabatic (isentropic) process, the entropy at the inlet of the turbine must be equal to the entropy at the outlet:

$$s_3 = s_{4s} \quad (21)$$

The losses in the turbine are primarily those related to the flow of the working fluid through the turbine. Heat transfer to the surroundings also represents a loss, but this is of usually of secondary importance. The governing procedures may also cause a loss in the turbine, particularly if a throttling process is used to govern the turbine. The losses associated with irreversibilities cause the turbine efficiency to deteriorate from the ideal.

The efficiency of a turbine (isentropic efficiency) is defied as:

$$\eta_s = \frac{h_3 - h_4}{h_3 - h_{4,s}} \quad (22)$$

The work done by a real turbine is calculated as:

$$W_T = \dot{m}(h_3 - h_4) \quad (23)$$

Heat transferred to the surrounding is not incorporated in the equation 23, as it is the less significant part. In case the heat transfer becomes significant, following equation should be used to calculated actual work done:

$$W_a = W_T - Q_L \quad (24)$$

Where, W_a presents the actual work done by the turbine and Q_L is the heat transfer to the surroundings.

The value of isentropic efficiency is calculated from a developed turbine map. It is reported by many authors i.e. (Erdem and Sevilgen 2006) that ambient temperature has a prominent effect on turbine performance. Therefore, the ambient temperature has been taken into account to develop the maps for this work:

$$\eta_s = \frac{a}{T_{amb}} + b.r_p + c \quad (25)$$

Where, T_{amb} is the ambient air temperature in *K*, r_p is the turbine pressure ratio (inlet to utlet), η_s is the isentropic efficiency and *a, b, c* are constants. Values of the constants are optimized using available plant operation data.

2.4 The recuperator model

The residence time of pentane in the recuperator is in the order of few minutes. Therefore, it can be assumed to have static characteristics. The heat transfer from the turbine outlet fluid to condenser outlet fluid is calculated from the following equation:

$$Q^{Rec} = U^{Rec} A^{Rec} \Delta t_m^{Rec} \quad (26)$$

Where, U^{Rec} is the overall heat transfer coefficient, A^{Rec} is the effective heat transfer area of the recuperator and Δt_m^{Rec} is the log mean temperature deference and calculated as:

$$\Delta t_m^{Rec} = \frac{(T_4 - T_2) - (T_{4a} - T_{2'})}{\ln \frac{(T_4 - T_2)}{(T_{4a} - T_{2'})}} \quad (27)$$

The value of the heat transfer coefficient is calculated using the following approximated equation:

$$U^{Rec} = U_S^{Rec} (\dot{m}_{2b} / \dot{m}_{2b,s})^{0.5} \quad (28)$$

Here, $\dot{m}_{2b}$ is the turbine outlet mass flow, U_S^{Rec} is the standard heat transfer coefficient and $\dot{m}_{2b,s}$ is the standard turbine outlet mass flow.

2.5 The condenser model

The ORC unit uses an air-cooled condenser. The following equation is used to calculate the outlet enthalpy:

$$h_1 = h_4 - \frac{Q_{con}}{\dot{m}_{2b}} \quad (29)$$

Modelling assumptions for the condenser are listed below:

- The mass flow rate is conserved.
- The minimum temperature of the condenser is 7°C more than the saturated temperature of the pentane at the prevailing pressure in the condenser.
- There is a minimum temperature difference of 8°C between the ambient temperature and the condenser outlet temperature to provide heat transfer from the pentane to the ambient air.
- Lumped heat capacity method was used for the calculation. The calculated Biot number of the fins is 8.4 X 10^{-6} . It is much less than 0.1, the criterion for such analysis (Holman 1992).

2.5.1 Calculation of heat transfer coefficient of horizontal inside tubes

The equations used to model heat transfer coefficients are taken from (Mueller 1992). The equation for heat transfer coefficient is calculated from the following equation of horizontal tubes assuming a stratified layer:

$$\alpha_i = \Omega \left[\frac{k_l^3 \rho_l (\rho_l - \rho_g) g \Delta h_v}{\eta_l d_i (T_{sat} - T_w)} \right]^{1/4} \quad (30)$$

Where, ρ_l is the density of fluid at a liquid state, ρ_g is the density of fluid at a vapour state, η_l is the dynamic viscosity, T_{sat} is the saturation temperature, T_w is the wall temperature and Δh_v is the change in enthalpy.

$$\Omega = 0.728 \left[1 + \left(\frac{1 - x_g}{x_g} \right) \left(\frac{\rho_g}{\rho l} \right)^{\frac{2}{3}} \right]^{-3/4} \quad (31)$$

2.5.2 Calculation of heat transfer coefficient of horizontal outside tubes

The condenser tubes have circular fins attached to them. While calculating the total heat transfer from a finned tube, one must take into account the heat transfer through the fins as well. The weighted heat transfer coefficient for the finned tube is:

$$\alpha_o A_t = \alpha (A_f \eta_f + A_r) \quad (32)$$

Where, A_r is the surface of the tube that is not covered by fins, A_f is the surface of the fin and A_t is the total surface area, $A_t = A_f + A_r$. The fin efficiency, η_f for the condenser tube is taken as 75%, which is a typical value.

The average Nusselt number for a finned tube in a bank with a staggered tube arrangement with the number of rows less than 4 can be calculated using following equation

$$Nu = 0.19 \left(\frac{a}{b}\right)^{0.2} \left(\frac{s}{d}\right)^{0.18} \left(\frac{h}{d}\right)^{-0.14} \mathrm{Re}^{0.65} \mathrm{Pr}^{0.33} \quad (33)$$

Where, $a = s_1 / d$, $b = s_2 / d$, s_1, s_2 are transverse and longitudinal bank pitch, and *s* is fin spacing. This equation is valid in the range $10^2 <$ Re < 2 X 10^4.

$$Nu = \frac{\alpha d}{k} \quad (34)$$

and

$$\mathrm{Re} = \frac{\rho w d}{\eta} \quad (35)$$

Where *d* is the tube diameter at the fin base and *w* is the maximum velocity of the fluid, which occurs at the minimum free cross section of the finned-tube bank (Figure 7).

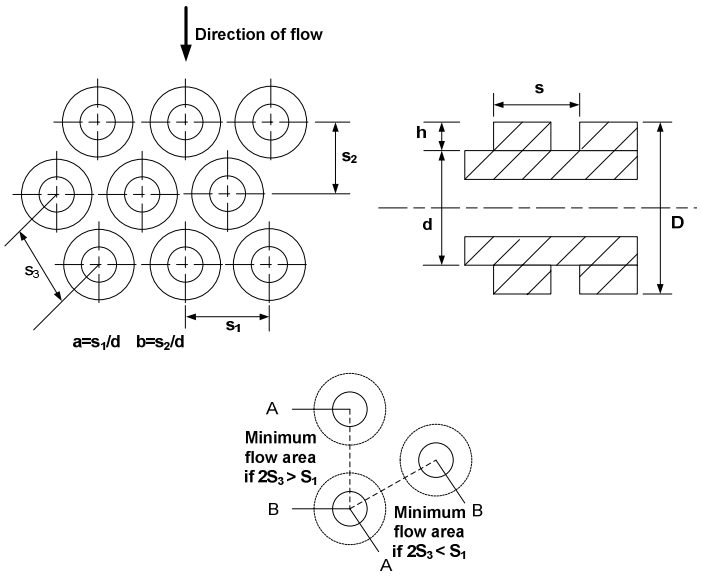

Figure 7: Definitions of quantities for flow in finned-tube banks.

The overall heat transfer from a finned-tube heat surface can be obtained using the following equation:

$$\frac{1}{U^C} = R_{fi}\left(\frac{A_t}{A_i}\right) + \frac{1}{\alpha_i (A_i / A_t)} + \frac{b_w}{k_w (A_{nb} / A_t)} + \frac{1}{\alpha_0} + R_{fo} \quad (36)$$

Where, R_{fi} = fouling resistance on the inside surface; A_i = inside surface area; A_{nb} = means the bare surface area; b_w = tube wall thickness; R_{fo}= fouling resistance on the outside surface.

The total amount of heat rejected from the condenser is calculated using the following equation:

$$\dot{Q}^C = U^C A_t^C \Delta t_m^C \quad (37)$$

Logarithmic mean temperature difference (LMTD) needed in the above equation is calculated as:

$$\Delta t_m^C = \frac{T_o - T_{amb}}{\ln\left[(T_w - T_{amb})/(T_w - T_o)\right]} \quad (38)$$

Where, T_o and T_{amb} are outlet and inlet temperatures of cooling air, respectively. T_w is the wall temperature and it is approximated with reasonably good accuracy as:

$$T_w = (9.T_{sat} + T_{amb})/10 \quad (39)$$

The fluid properties are evaluated at an average (bulk) temperature:

$$T_b = \frac{T_1 + T_{4a}}{2} \quad (40)$$

In equation 38, the outlet temperature of air, T_o is not known and is calculated iteratively. As an initial guess, T_o is taken to be the same as T_w. From the air side energy balance the heat transfer rate can be calculated:

$$\dot{Q}^C = U^C A_t^C \Delta t_m^C = \dot{m} Cp(T_o - T_i) \quad (41)$$

The initial LMTD can be calculated using the above mentioned equation. From this value of LMTD a refined value of T_o can be calculated iteratively, using equation 38. Finally, using the obtained T_o, a better approximation of LMTD is obtained.

Free convection occurs at the headers (where condenser tubes are connected in bundles at the inlet and outlet) of the condenser and pipeline from the condenser to the recuperator. However, it was found that the quantity of heat transfer is very low (approximately 0.05%) compared to that of the condenser itself. Therefore, the effect of heat transfer through headers and pipeline are not taken into consideration. The simplified equation for free convection from a horizontal cylinder surface to air at atmospheric pressure under laminar flow condition was used for the analysis (Holman 1992).

The outlet temperature of the header depends on the holdup mass in the header and is calculated from the following equation:

$$M^C \frac{T_1}{dt} = \dot{m}_P (T_1^{'} - T_1) \quad (42)$$

Here, c_p is assumed to be constant, therefore is cancelled out from both sides of the equation. M^c represents the holdup mass in the condenser header and $T_1^{'}$ presents pentane inlet temperature to the condenser header and calculated using h_1 and saturation pressure.

2.5 The cycle pump

It was found for the designed values, the ratio between the total enthalpy of pentane at the cycle pump outlet and the combined heat input at the recuperator and the vaporizer is about 1.03%, which implies that the effect change of pump output pressure (enthalpy) is insignificant compared to the total heat input. Therefore, the pump work can be assumed constant (Wei et al. 2007). The pump outlet pressure has been fixed at 23 bar for the simulation carried for this work. Moreover, the pump is also assumed to have static characteristics same as the turbine because of its fast response.

2.6 The pressure drops in pipes and valves

The pressure drops in various valves are assumed negligible. The valves operating in the pentane cycle include the vaporizer pentane-level control valve, situated between the cycle pump and the vaporizer, and the flow control valve situated just after the vaporizer and the turbine inlet. In a typical operation of the plant, the flow control valve is set to its maximum and therefore its effect can be ignored.

There are a few other valves attached to the unit, which are not used in normal operation of the plant. Such valves include the bypass valve from the vaporizer to the condenser and the valve for the purge system. The bypass valve is a safety system and only operates in emergencies. The purge systems are actuated when backpressure builds up in the condenser. Although there is an automated purge system working in the unit, its response is very slow and most of the time it is done manually. Therefore, it is beyond the scope of this work.

For flow through pipes, there exist major and minor losses (Potter and Wiggert 2002). For simplicity of the model, only major losses are considered:

$$h_{loss} = f \frac{l}{d} \frac{v^2}{2g} \quad (43)$$

However, an easy to use model for pressure drop (Wei et al. 2008) has been adopted for the modelling:

$$\frac{\dot{m}}{\dot{m}_s} = \sqrt{\frac{\Delta p}{\Delta p_s} \cdot \frac{\rho}{\rho_s}} \quad (44)$$

Here, suffix *s* stand for standard or observed value.

2.7 The turbine-generator coupling

A generator is coupled to the turbines and has heavy rotating parts. However, in normal operations, the generator is maintained at a constant speed so the effect of the inertia of angular velocity does not affect the electrical power output. With a change in thermal power output, the speed of the generator changes and there is a control arrangement to adjust its speed. The target speed for this generator is 1500 rpm. The change in electrical power output is the sum of

change of thermal power output and change of angular momentum of the generator shaft:

$$\frac{dP_{el}}{dt} = \frac{d}{d\tau}(\eta_{el}.P_{th}) + \frac{d}{d\tau}(\frac{1}{2}I\omega^2) \quad (45)$$

Where, P_{el} is the electrical power output, P_{th} is the thermal power output, η_{el} is the electrical energy conversion efficiency and assumed to be constant, I is the mass moment of inertia and ω is the angular velocity. It is easy to show from the above equation that:

$$P_{el} = \eta_{el}.P_{th} + \frac{1}{2}I(\omega^2 - \omega_0^2) \quad (46)$$

Where, ω_0 is the angular velocity at time, $t= 0$. Now, it is known that electric power produced in a generator is proportional to its angular velocity:

$P_{el} \propto \omega$, or,

$P_{el} = k\omega$,

or $\omega = \frac{P_{el}}{k}$ (47)

Putting this value in equation 46 one gets:

$$P_{el} = \eta_{el}.P_{th} + \frac{1}{2}I(\frac{P_{el}^2}{k^2} - \omega_0^2) \quad (48)$$

2.8 Results and discussion

The simulation was carried out for 1000 hours of operation of the power generating unit. The ambient temperature and the brine mass flow rate were supplied to the model and it predicted the performance of ORC unit accordingly. Figure 8 summarises the ambient temperature for the 1000 hours of operation. The ambient temperature has both daily change and seasonal change. The seasonal change in temperature is easily understood from the Figure 8. To show how ambient temperature changes over a typical day, a magnified view of the marked area is presented in Figure 9. The condenser performance is directly related to the ambient temperature and consequently the electrical power output. Further discussion is presented later in this section. Figure 10 summarises the brine mass flow rate used for the simulation. Both the ambient temperature and the brine flow rate are actual values of an hour interval for 1000 hours of operation of the plant.

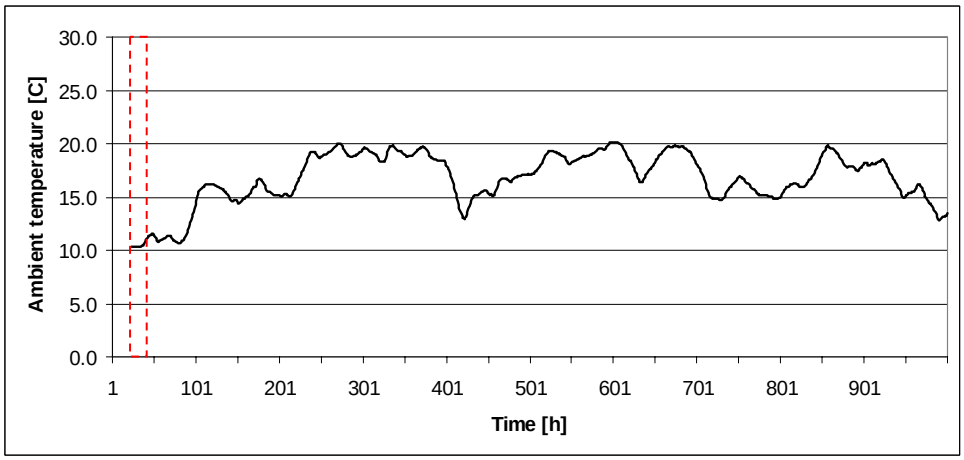

Figure 8: Ambient temperature of the plant vicinity for 1000 hours of operation of the ORC unit (averaged 24 hours).

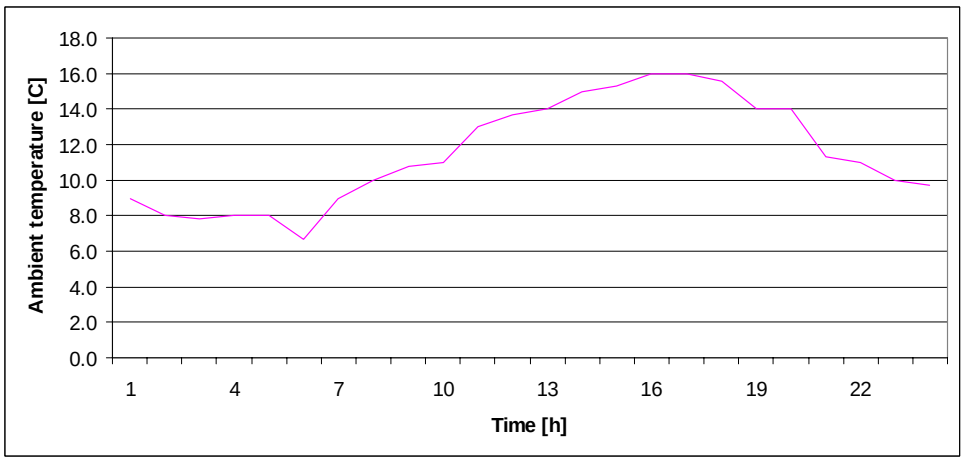

Figure 9: Ambient temperature of the plant vicinity for a day operation of the ORC unit.

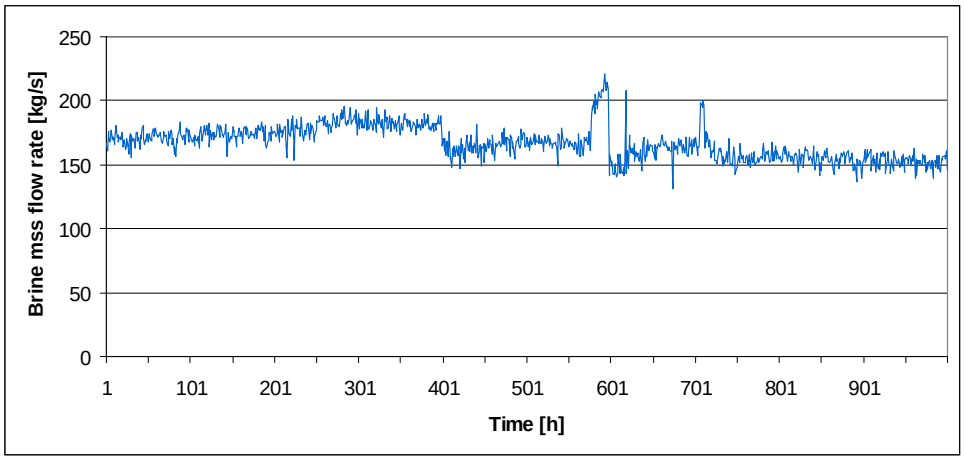

Figure 10: Brine mass flow rate for 1000 hours of operation of the ORC unit.

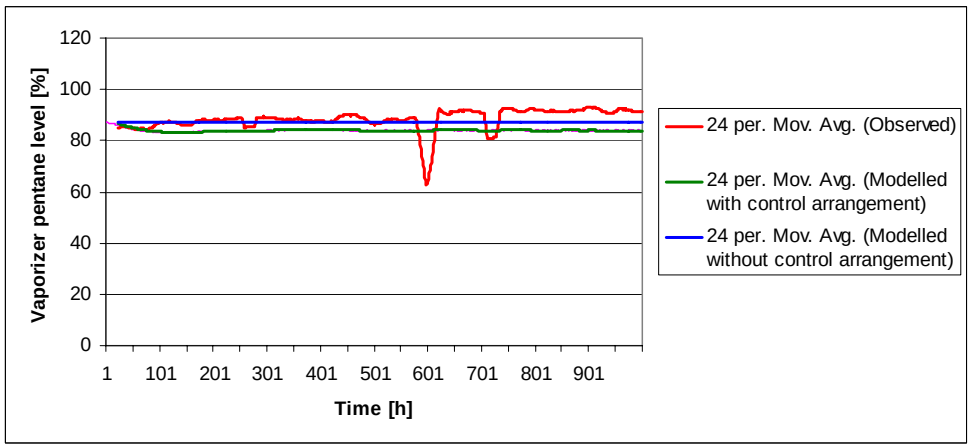

Figure 11: Vaporizer pentane level for 1000 hours of operation of the ORC unit

2.8.1 The vaporizer pentane level

The pentane level in the vaporizer plays a very significant role in the system dynamics. There is a feedback control mechanism to control the pentane level. An operator gives a set point (reference value) from the key board as judged appropriate depending on their experience. Once a set point is provided, it takes about 10-15 minutes for the controller to change the pentane level from its original to the new set point. After the controller takes over, the pentane level does not change significantly. The controller does not take into account the flow rate of the pentane outlet of the vaporizer directly but measures the pentane level. The pentane mass flow is a direct consequence of the of the heat transfer from the brine to the pentane in the vaporizer and the quantity of heat transfer is dependent mainly on the brine flow rate as the brine is fed at a constant temperature. The brine flow rate has changed significantly over time from the designed value or even from the state when the plant was first built. In case of abrupt change in the brine mass flow, the operators change the pentane level's set point and there is also a control mechanism which bypasses the pentane vapour in case of a sudden increase in pentane vapour generation. A PID Simulink block has been used (P=0.8; I= 0.01; D= 0.01) as the controller.

If the level control mechanism works properly, other than from the effect of sudden change in brine mass flow, the pentane level in the vaporizer can be assumed to have an insignificant effect. Figure 11 compares the actual pentane level, the pentane level with the feedback control having its level set point at 84% and the pentane level without feedback control. It can be seen from Figure 11 that, at about 75 hours of operation of the unit, the model with feedback control gives a better match with the actual value. However, over time, it changes and the model without the feedback controller gives a close match. By choosing an appropriate value of the set point of the pentane level, the feedback control will eventually give a better result than the model without feedback control. However, a feedback loop is associated with a long simulation time and clumsy calculations. As can be seen from the Figure, the difference in result between the model without feedback control and the actual is not very significant and it can be assumed that the control mechanism is in use and it makes the pentane level follow a set point. This will save a lot of calculations and consequently computation time at the expense of accuracy. Nonetheless, the model without feedback control produces reasonably accurate results. All the results of simulation presented in this section use no feedback control for the vaporizer pentane level.

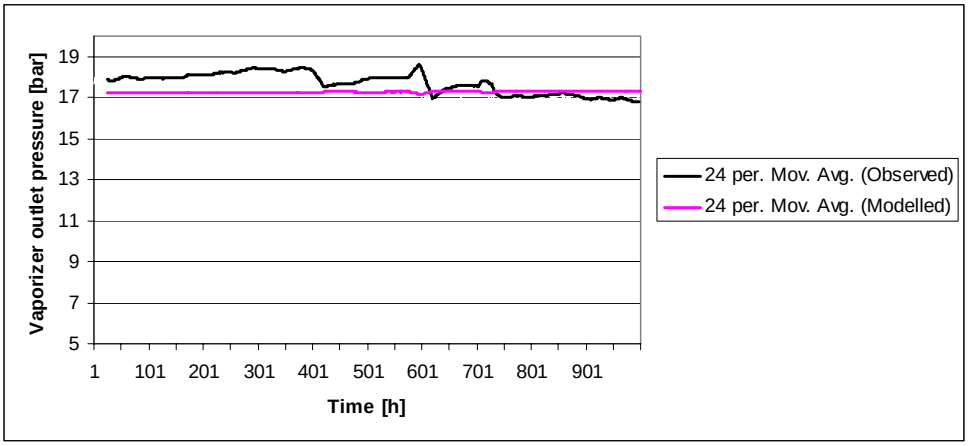

Figure 12: Vaporizer outlet pressure for 1000 hours of operation

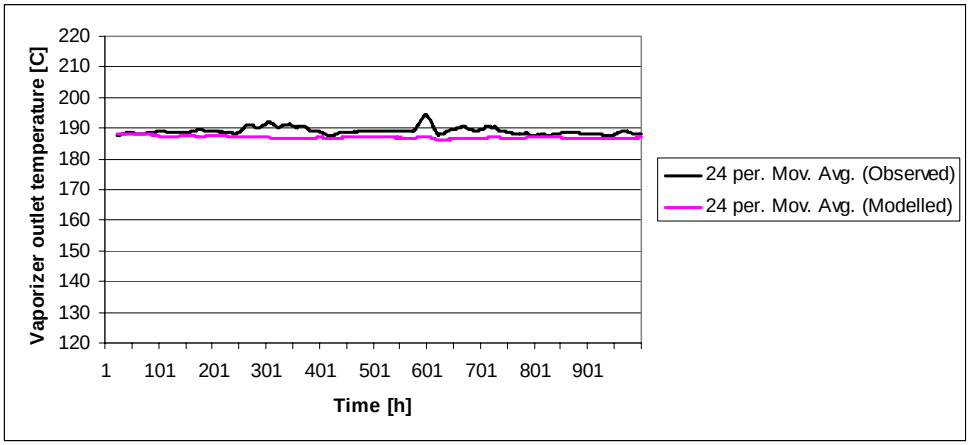

Figure 13: Vaporizer outlet temperature for 1000 hours operation

2.8.2 The vaporizer outlet pressure

Figure 12 presents the observed and modelled vaporizer outlet pressure for 1000 hours of operation of the vaporizer. A reasonably close match is easily perceived and the average percentage error is found to be 3.5%. The maximum value of percentage error is quite high (9.27%), and this occurred due to abrupt change in the mass flow of brine. This error occurred at 579 hours of operation which is the peak of a sudden change of mass flow (Figure 10). There were two big peaks of sudden mass flow change at around 580 hours and 700 hours that stayed for a while. These two peaks had a significant effect on the simulation results whereas they do not have the same significant effect on actual operations as these peaks are normally tackled by operators by changing the pentane level, bypassing excess pentane to the condenser, operating the purge system of the condenser manually, and the speed control system of the turbines etc. Therefore, the inability to control these peaks can be considered as a limitation of the developed model. Further models can be developed with capabilities to manage the effect of sudden change; however, the main idea of modelling the power plant is to predict future plant performance depending on geothermal resources and weather. With sudden changes in resource characteristics and weather, plant operators can take over the control from the automatic control. The legitimacy of not developing a model with ability to tackle sudden changes relies on it.

2.8.3 The vaporizer outlet temperature

Figure 13 shows the observed and the modelled pentane temperatures at the vaporizer outlet. The average percentage error is found to be 1.1% and the percentage error has a maximum value of 5.14%. A good match between the actual and the modelled vaporizer temperatures is very important. The state of the pentane vapour (p, T, h) at the vaporizer outlet dictates how much energy is available to produce power as the turbine outlet pressure is given to the model externally. In actual plant operation, the turbine outlet pressure does not change much and it is related to the condenser pressure.

2.8.4 The electric power output

Figure 14 presents the comparison of the actual and modelled electric power output from the ORC unit. It is evident from the figures (14-15) that the developed model is capable of predicting both daily and seasonal load changes. The average percentage error is 4.8%. All error is calculated as absolute value and the maximum value of percentage error is very high (31.46%). This error occurred at 619 hours of operation for the same reason as discussed in previous paragraphs. There are two peaks of brine mass flow at about 579 and 720 which are taken care of by operators and the control mechanism in place in actual plant operations. The error in vaporizer outlet temperature however, was not much affected by this sudden change in brine mass flow; the main reason behind it is that the dynamics of temperature change

are associated with very large mass (pentane mass itself, vaporizer mass, separator mass, pipes mass, condenser mass etc.) and it is much slower than the dynamic of the turbine. Nonetheless, the model is very competent in predicting performance in normal operations of the plant and if a saturation block is used which limits mass flow rate to imitate the bypass mechanism, the performance of the model can be improved (Figure 16). The average percentage error is 4.5% and the maximum value is 27.18%.

2.8.5 The condenser outlet temperature

Figure 17 presents the condenser outlet temperature of the unit for 1000 hours of operation. It is very clear from the Figure that the modeled condenser outlet temperature follows the observed values very competently. However, the temperatures are measured in °C and are low. Therefore, the relative errors are high. The average of percentage error is 10%, but if we use temperature in absolute scale, the average percentage error would be very low 0.89%, with the maximum values of percentage error is 4.03%.

2.8.6 The brine outlet temperature

Figure 18 shows the observed vs. modelled brine outlet temperature and a close match between the two values is clear. The average percentage error is 1.43% and the maximum value is 6.90%. All error is calculated as absolute value and it can be seen from the Figure that the typical value of the brine outlet temperature is about 140°C.

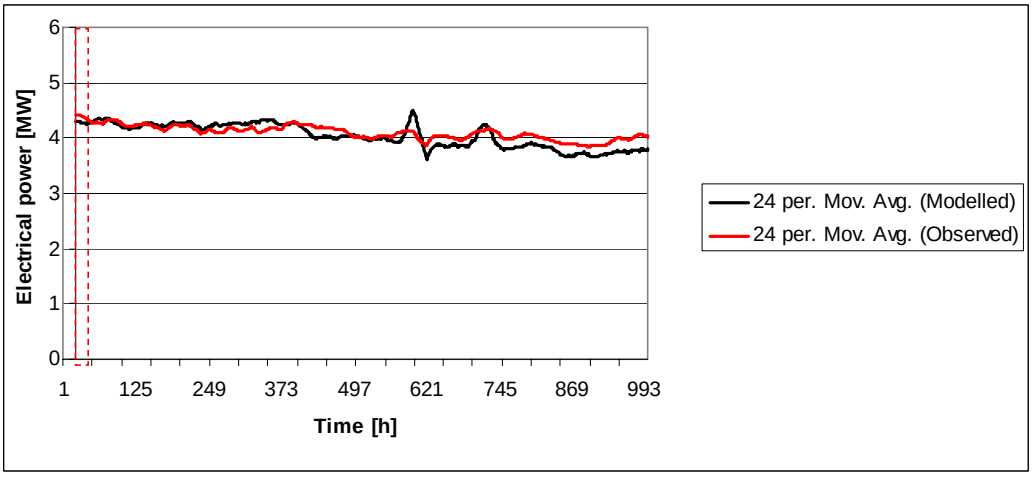

Figure 14: Electrical power output for 1000 hours of operation

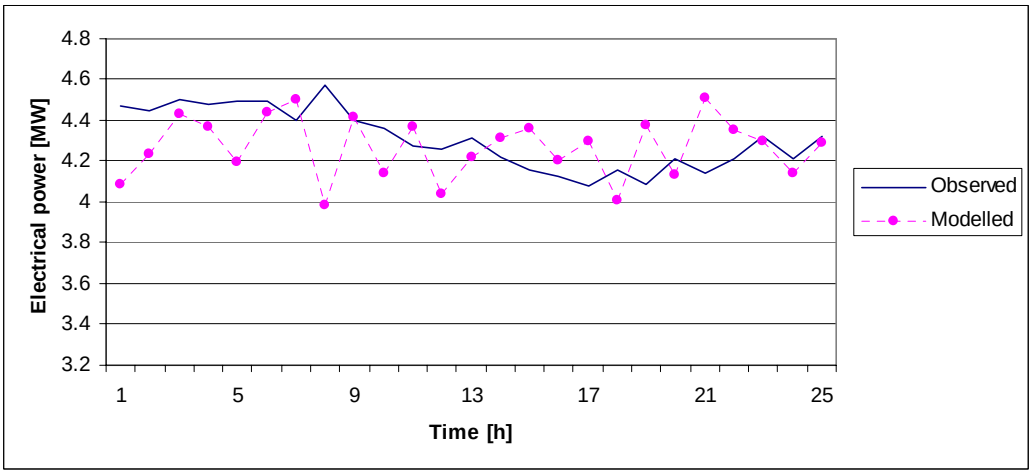

Figure 15: Electrical power output for a day's operation

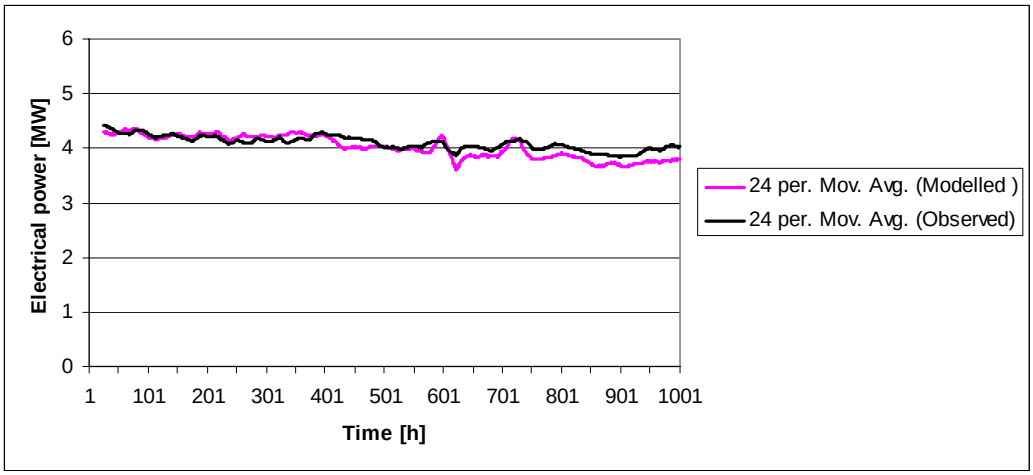

Figure 16: Electrical power output for 1000 hours of operation with a maximum pentane mass flow of 48.5 kg/s

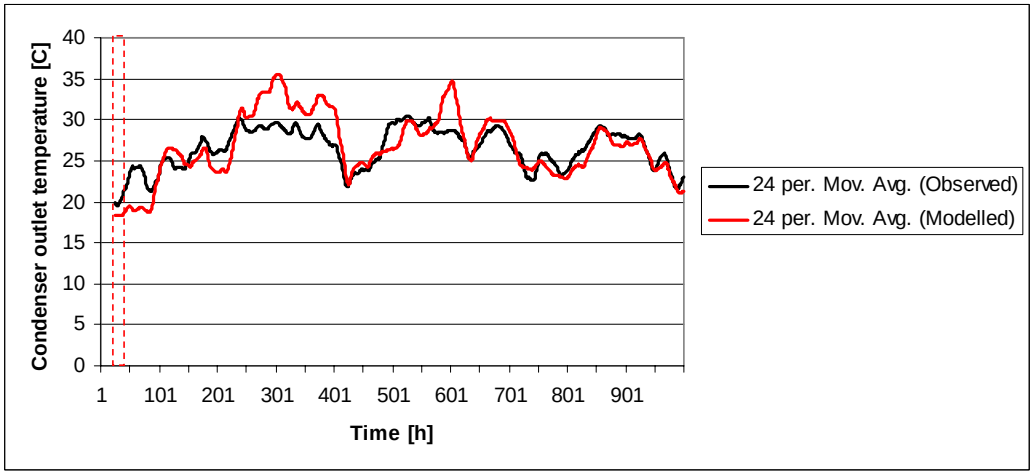

Figure 17: Condenser outlet temperature for 1000 hours

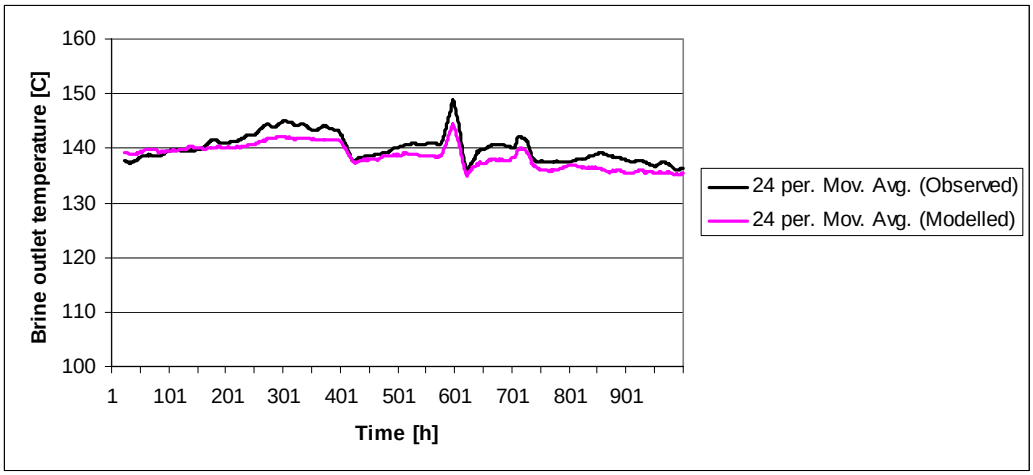

Figure 18: Brine outlet temperature for 1000 hours operation

2.9 Conclusions

Steady state model of geothermal power plants are commonly available in the literature. However, dynamic models are not very common. In this paper a dynamic model of an ORC unit of a geothermal power plant is presented. The model takes into account effect of internal and external parameters, which are necessary to simulate the plant performance with reasonable accuracy. The results of simulation are also presented and compared against the plant performance data. It was found that the developed model is competent to predict the plant performance with reasonably high accuracy. The average percentage error of electric power output remains within 5%.

REFERENCES

Bai, O., Nakamura, M., Ikegami, Y., and Uehara, H. (2004). "A Simulation Model for Hot Spring Thermal Energy Conversion Plant With Working Fluid of Binary Mixtures." *Journal of Engineering for Gas Turbines and Power*, 126(3), 445-454.

Casella, F. (1999). "PhD Thesis: Modelling, Simulation, and Control of a Geothermal Power Plant," PhD, POLITECNICO DI MILANO, MILANO.

Erdem, H. H., and Sevilgen, S. H. (2006). "Case study: Effect of ambient temperature on the electricity production and fuel consumption of a simple cycle gas turbine in Turkey." *Applied Thermal Engineering*, 26(2-3), 320-326.

Holman, J. P. (1992). *Heat Transfer*, 7 Ed., McGraw-Hill.

Jurado, F., Cano, A., and Carpio, J. (Year). "Enhancing the Distribution System Stability Using Micro-Turbines and Fuel Cells." *Proceedings of the IEEE Power Engineering Society Transmission and Distribution Conference*, 717-722.

MathWorks. (2008). "www.mathworks.com."

Mattsson, S. E., and Siiderlind, G. (1993). "A New Technique for Solving High-Index Differential-Algebraic Equations Using Dummy Derivatives." *SIAM journal on scientific computing* 14(3), 677-692

Mueller, A. C. (1992). *Hand Book of Heat Exchanger Design*, Begell House, Inc.

Nakaoka, T., and Uehara, H. (1988). "PERFORMANCE TEST OF A SHELL-AND-PLATE TYPE EVAPORATOR FOR OTEC." *Exper Therm Fluid Sci*, 1(3), 283-291.

Potter, M. C., and Wiggert, D. C. (2002). *Mechanics of Fluids*, 3rd Ed., Bill Stenquist.

Pritchard, G. (2002). "The must-run dispatch auction in an electricity market." *Energy Economics*, 24(3), 199-216.

PSE. (2008). "Process Systems Enterprise Ltd. http://www.psenterprise.com/."

REFPROP. (2007). "National Institute of Standards and Technology (NIST), http://www.nist.gov/." <http://www.nist.gov/>.

Wei, D., Lu, X., Lu, Z., and Gu, J. (2007). "Performance analysis and optimization of organic Rankine cycle (ORC) for waste heat recovery." *Energy Conversion and Management*, 48, 1113–1119.

Wei, D., Lu, X., Lu, Z., and Gu, J. (2008). "Dynamic modeling and simulation of an Organic Rankine Cycle (ORC) system for waste heat recovery." *Applied Thermal Engineering*, 28(10), 1216-1224.